

Spectroscopy Letters

An International Journal for Rapid Communication

ISSN: 0038-7010 (Print) 1532-2289 (Online) Journal homepage: <https://www.tandfonline.com/loi/lstl20>

Near-infrared methane sensor based on a distributed feedback laser

Jianing Wang, Bin Li, Guanyu Lin, Qingjun Ma, Shurong Wang & Mingxu Piao

To cite this article: Jianing Wang, Bin Li, Guanyu Lin, Qingjun Ma, Shurong Wang & Mingxu Piao (2019): Near-infrared methane sensor based on a distributed feedback laser, Spectroscopy Letters, DOI: [10.1080/00387010.2019.1569063](https://doi.org/10.1080/00387010.2019.1569063)

To link to this article: <https://doi.org/10.1080/00387010.2019.1569063>



Published online: 05 Feb 2019.



Submit your article to this journal [↗](#)



Article views: 3



View Crossmark data [↗](#)



Near-infrared methane sensor based on a distributed feedback laser

Jianing Wang^a, Bin Li^b, Guanyu Lin^a, Qingjun Ma^a, Shurong Wang^a, and Mingxu Piao^c

^aChangchun Institute of Optics, Fine Mechanics and Physics, Chinese Academy of Sciences, Changchun, Jilin, China; ^bInstitute of Electrical & Computer, Jilin Jianzhu University, Changchun, Jilin, China; ^cDepartment of Optical Engineering, Changchun University of Science and Technology, Changchun, Jilin, China

ABSTRACT

In this article, a near-infrared methane detection system using tunable diode laser absorption spectroscopy technology was designed and implemented. The distributed feedback laser was driven by a self-developed temperature and current controller to allow scanning the selected absorption wavelength at 1654 nm. Laser temperature fluctuation was lower than 0.01%, and the output emission wavelength was linear and stable. The emitted beam passed a reflective gas chamber and was received by the Indium Gallium Arsenide photodiode detector. Through a data acquisition card, a digital lock-in amplifier was developed to extract the second harmonics with real-time monitoring and adjustment. Based on Allan deviation analysis, the limit of detection was about 48 ppm with a path length of 30 cm, at an integration time of 6 s. The experimental results revealed a maximum detection error of less than 3% at a gas concentration higher than 100 ppm. The fluctuations rates in long-term (9 hr) stability measurements for 1×10^3 ppm and 1×10^4 ppm methane samples were 0.8% and 0.48%, respectively, indicating good stability for the sensor. In the control module design, compared with previous reports on methane detection systems, the current system uses a self-developed temperature controller, a current driver and a signal processor, to allow real-time display and adjustments. The potential for adjustable wavelength scanning is available for multi-gas detection based on a single detection system.

ARTICLE HISTORY

Received 23 October 2018
Accepted 9 January 2019

KEYWORDS

Absorption spectrum;
distributed-feedback; lasers

Introduction

Methane is the second most important anthropogenic greenhouse gas after carbon dioxide, and its levels have increased from a pre-industrial average atmospheric mole fraction of about 722 parts per billion (ppb) to 1833 ± 1 ppb in 2014, an increase of 9 ppb compared with the previous year.^[1,2] As an inflammable and explosive gas, the urgent requirements of avoiding safety hazard in environmental science, public safety, and industrial monitoring are becoming a driving force for the development of real-time, efficient, and robust methane sensor systems. Different applications have called for the development of sensitive, accurate, robust, and *in-situ* methane sensor systems.^[3–4]

Existing traditional methane sensing techniques, including electrochemical,^[5] catalyst combustion,^[6,7] and semiconductor^[8,9] methods, normally have some application limitations such as insufficient detection accuracy, poor selectivity, and strict requirements for application environment. Even though detection performance can be satisfactory by applying conventional mass spectrometry or gas chromatography,^[10] the relatively large size, long resolution time, and complicated pretreatment limit real-time *in-situ* methane detection. Compared with the traditional detection devices mentioned above, the infrared optical detection technology^[11–13] offers desired advantages, including fast response, high precision,

and is favored in current researches. In order to achieve precise measurements of low concentrations, a high signal-to-noise ratio (SNR) is considered a significant optimization indicator. In the infrared optical detection technology, the tunable diode laser absorption spectroscopy (TDLAS) technology as a non-contact detection method suitable for *in-situ* detection is effective for trace gas detection.^[14–16] Kinds of laser sources, such as fiber laser and diode laser,^[15,16] are applied to the *in-situ* environment gas concentration detections with the application of fiber laser technology.^[17] Generally, detection performance is limited by the laser driving circuit, selected absorption length and matched signal processing system.^[18] Therefore, the newly developed sensor focused on improving (1) the temperature control performance, (2) second-order harmonic extraction performance, and (3) application ability in *in-situ* environments. In addition, a multi-pass gas chamber and a dual-channel detection method were adopted to effectively enhance light absorption efficiency and suppress environmental influences.^[19]

First, for the selection of absorption lines, most gas molecules, such as methane carbon dioxide and water, have strong absorption in the mid-infrared spectral range. Theoretically, detection performance using quantum cascade lasers (QCLs) in the 4–12 μm spectral range,^[20] and that of interband cascade lasers (ICLs) in the 2.5–6 μm range^[21] can achieve

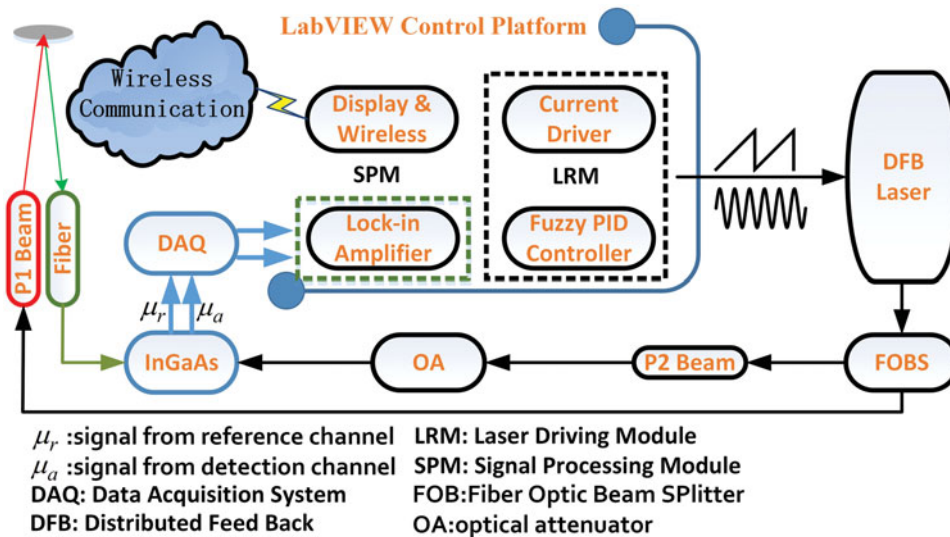


Figure 1. Structure of the methane detection system. Methane detection system based on tunable diode laser absorption spectroscopy technology was controlled by self-developed LabVIEW platform.

satisfactory performance. However, the high cost of lasers and strict working conditions limit the *in-situ* application of sensors using QCL and ICL lasers in some industrial areas such as fine agriculture. Considering the actual application demand, distributed feedback (DFB) lasers using the WMS technology is recommended to overcome the abovementioned drawbacks.

Secondly, a driving signal module and signal processing module are designed and implemented, matching the wavelength modulation spectroscopy (WMS) technology^[22] to achieve satisfactory detection performance and flexible application. Currently, traditional temperature control modules are designed based on a simple PID controller on a DSP chip, and there is still room for improvement in terms of performance.^[23] In addition, somewhat satisfactory temperature control performance (about $\pm 0.01^\circ\text{C}$ fluctuation) could be achieved at the cost of long response time (longer than 60 min)^[24] In this article, a Fuzzy PID controller was designed to improve control accuracy from $\pm 0.1^\circ\text{C}$ to $\pm 0.018^\circ\text{C}$ ^[23] and decrease response time to 9 s. Besides digital control, the self-developed digital orthogonal lock-in amplifier simplifies the complexity of input signals compared to phase-tuned-type lock-in amplifiers. Based on a high sample frequency and a digital low pass filter, the extraction error was less than 0.77%.

Thirdly, the control modules were designed based on the LabVIEW platform with visible inputs and outputs to replace detection systems with fixed parameters.^[25,26] Adjustable driving parameters and a laser with required central wavelength have a potential to detect different gases using the same control platform. In addition, both the hardware cost and sensor size were effectively reduced.

Overall, a methane detection system based on the TDLAS-WMS technology was implemented and experimentally demonstrated. A control terminal designed on the LabVIEW platform realizes the functions of both laser driving and signal processing. The rest of this article is organized as follows. In the *Methane sensor configuration and theory* section, the detection structure and theory were described, including absorption spectroscopy selection and the modulation method. Then in *Design of the driving and signal processing circuit* section,

sensor fabrication details and related experiments were presented to indicate the modulation performance, including temperature control, current modulation, and harmonic signal extraction using a digital orthogonal lock-in amplifier. Next, in *Experiment and calibration* section detection performance was evaluated based on gas experiments. Finally, the article ends with some discussion and conclusion.

Methane sensor configuration and theory

Sensor structure

A schematic representation of the methane detection system is shown in Fig. 1. The whole control module realized on the LabVIEW platform could be separated into two main parts, including DFB laser driving- and signal processing parts. The DFB laser driving signal was generated by a 5-kHz sine wave superimposing a 10 Hz saw tooth wave, and sent to the matched self-developed hardware driving circuit to drive the DFB laser. The emitting beam of the laser was split by a fiber optic beam splitter (FOBS) for differential detection. In the signal processing part, two power-equivalent beams directly fiber-linked to the photodiode (PD) module via an optical attenuator (OA) are received and identified as detection and reference signals, respectively. The OA is used to adjust the optical intensity of reference channel matching the detection channel. To ensure the adjustment accuracy, the resolution of selected OA is less than 0.2 dB. Meanwhile, the two channel signals are sampled and transformed on the LabVIEW platform for subsequent digital signal processing. Furthermore, the instrument based on the LabVIEW platform has a potential to be a wireless sensing node with an embedded microprocessor and integration of suitable wireless communication components.

Absorption spectroscopy selection

In the spectroscopy selection, the radiation beam should satisfy the frequency selection characteristics of the gas

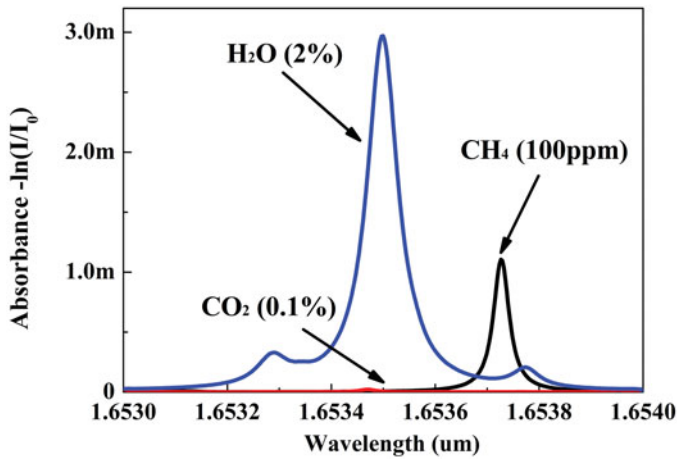


Figure 2. Absorption spectra around selected methane absorption line for interference gas analysis. HITRAN based absorption spectra of detection gas (100 ppm methane) and potential influential gases (2% water and 0.1% carbon dioxide) around absorption wavelength.

molecules, and the relationship between transmitted intensity $I(\lambda)$ and incident intensity $I_0(\lambda)$ follow Lambert's law as formula 1:

$$\tau(\lambda, t) = \frac{I(\lambda)}{I_0(\lambda)} = \exp[-\alpha(\lambda, t)LC] \quad (1)$$

where $\alpha(\nu, t)$ is the absorption coefficient at a specific absorption wavelength λ , C is the mole fraction of the detected molecule species and L is the absorption length which is equal to two times the chamber length in the actual design.

According to the theoretical analysis above, a suitable absorption wavelength for detecting methane should be selected before driving circuit implementation. Considering the trade-off between cost and measurement performance, an absorption peak at a wavelength of 1.65 μm was selected. Based on the high-resolution molecular spectroscopic database (HITRAN type of 2012), the absorption spectra of 100 ppm methane, water, and carbon dioxide derived at 1 atm gas pressure and unit optical path length are depicted in Fig. 2. An obvious methane absorption spectrum peaking at about 1.6537 μm could be scanned by the selected DFB laser. Water and carbon dioxide are two potential influential gas components in the application environment. At the same concentration, the absorption strengths of carbon dioxide and water at $\sim 1.6538 \mu\text{m}$ were at least four times weaker compared with methane absorption intensity. However, when environmental humidity was increased to 2%, interference from water became prominent as shown in Fig. 2. Therefore, in the gas cell, a water-proof coverage and an inside water trap based on calcium sulfate were used to minimize the effect of water on methane detection. Considering the application requirement and spectra lines, the scan band used in the TDLAS technology was from 1.6535 to 1.6541 μm .

Wavelength modulation

In near-infrared range, the detecting gas has an insufficient absorptive strength which limits the detection sensitivity and

lower limit of detection. In order to improve the performance of detection system, a WMS is used to reduce the $1/f$ noise.

In the implementation process, the DFB laser is tuned with a high-frequency sine wave signal with an angular frequency of ω_{sin} superimposed on a repetitive ramp waveform with a frequency of F_{ramp} . The frequency of ω_{sin} is 5 KHz as a carrier which is generated by a DDS chip (AD9852). In addition, a square wave is generated synchronously and transmitted to the signal processing terminal as a reference signal which has the same frequency and phase as the driving signal ω_{sin} . The frequency of F_{ramp} is 10 Hz which is used to scan the selected absorption line. Based on the difference between the periodicity of modulation signal and the randomness of noise, the harmonics signal is able to be extracted by the cross correlation calculation which is used to measure the gas concentration.^[27] The modulation signal is represented in formula 2.

$$u(t) = a \sin(\omega_{\text{sin}} t) + b F_{\text{ramp}}(t - F_{\text{ramp}}) + c \quad (2)$$

In this equation, a and b are constant amplitude factor, c is the DC offset.

The laser current is modulated and this results an intensity response as shown above in formula 3:

$$I(t) = I_0 \left[1 + m \mu_{\text{ramp}}(t) + m \mu_{\text{sin}}(t) \right] \quad (3)$$

The factor is the light modulation coefficient and is the average intensity at center frequency. The $\mu_{\text{ramp}}(t)$ and $\mu_{\text{sin}}(t)$ are the ramp signal and the sine signal, respectively.

Digital orthogonal lock-in amplifier

In view of the requirement of weak signal detection, the differential detection technology is used to further improve the signal to noise ratio. The output beam after absorption is separated by a splitter to detection signal and reference signal with same amplitude coefficient. The detection signal and reference signal are transmitted through the absorption chamber and attenuated directly, respectively. After the optical-to-electrical conversion, the signal is sampled by a DAQ and the digital output is transmitted as the input to a self-developed digital orthogonal lock-in amplifier based on LabVIEW. Based on a relative lower priority thread in kernel, the extracted first harmonic and second harmonic are used to match the absorption peak and calculated measuring gas concentration, respectively.

Open reflective gas cell

In the optical part, two FC/APC fiber interfaces connectors are used as the input and output for receiving the incident light beam. The self-developed cylindrical gas cell owns a compact structure with a 15 cm length and 3 cm diameter. This simple optical structure effectively decreases the cost and ensures the flexibility for special application in harsh environment. The mirror is located at the bottom to double

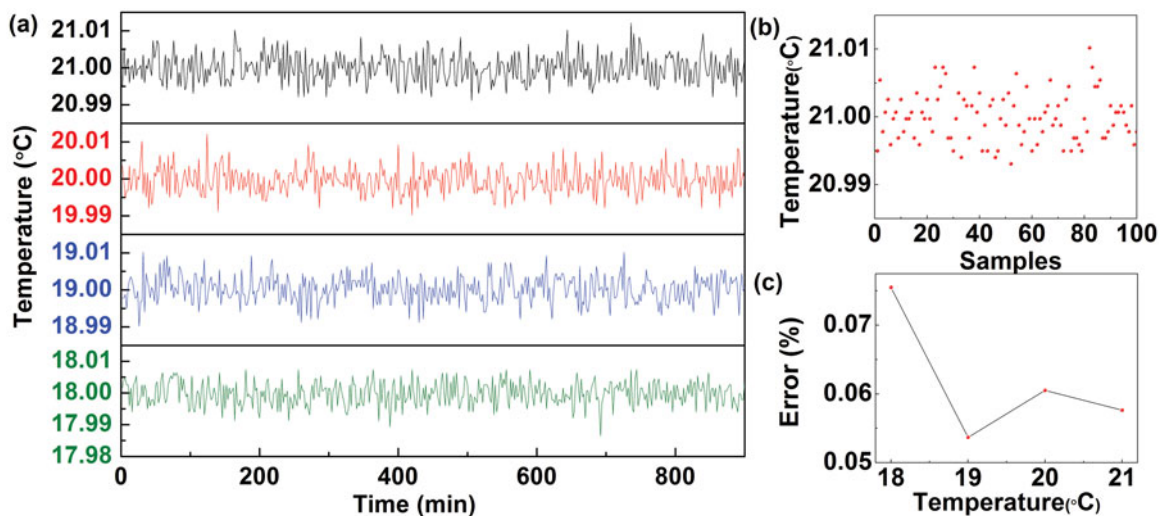


Figure 3. Temperature control performance test. Temperature stability test in 15 hr at range (a) from 18°C to 21°C; (b) temperature fluctuation at 21°C in detail and (c) error of measured temperatures.

the path length by reflecting the input optical beam and the output signal is received as a detection signal.

Design of the driving and signal processing circuit

Temperature controller

To drive the DFB laser in scanning the measuring absorption spectra, the temperature and driving current are the two main regulatory parameters. In the modulation process, the temperature is preferred for locking the center wavelength. The integrated DFB laser used in this design was a 14 pin butterfly-packaged with a thermoelectric cooler (TEC) module. In order to set up a closed-loop temperature regulation, a fuzzy PID control on the LabVIEW platform was designed and implemented. Through a DAQ and a DAC, the direct output to the TEC control pin is an analog voltage value. What's more, an inside-packaged thermistor with negative temperature coefficient (NTC) can achieve voltage value sampling. In the design of the fuzzy PID controller, a manual PID control and a fuzzy PID control are optional for different control requirements.

Considering the significance of temperature control, experiments were carried out to evaluate control performance parameters, including stability and precision. An external analog to digital converter was used to sample the feedback temperature value. The temperature was set from 18°C to 21°C simulating the actual modulation temperature with 1°C increase per step. The experimental results are shown in Fig. 3, lasting about 15 hours. Fig. 3a shows the temperature measurement results in different settings, and detailed fluctuations are shown in Fig. 3b. The fluctuations of four measurement temperature points were all less than 0.01% as shown in Fig. 3c, ensuring the performance of wavelength scanning. In addition, the response time taken during the temperature changing from an initial temperature to the of target temperature (fluctuation is less than 5%) was shorter than 9 s.

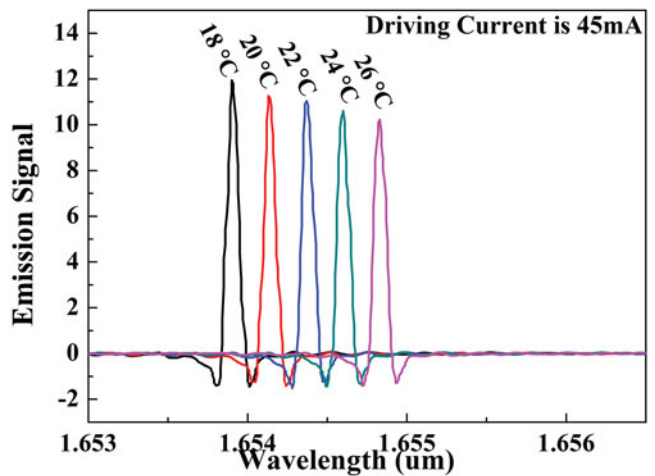


Figure 4. Emission spectra results under different temperature. Emission spectra with the temperature increasing by two degree from 18 to 26 degrees under 45 mA driving current.

The DFB laser has a center wavelength about 1.654 μm indicating a suitable temperature and current modulation are required to target the selected methane absorption line. In the actual design and implementation, the temperature control performance of this laser is able to be guaranteed when the operation temperature is between 16°C and 30°C without any air or water cooling devices. The output spectra were assessed using a Fourier Transform Infrared Spectrometer (Thermo Scientific, NICOLET 6700 FT-IR), as shown in Fig. 4. The injected current is locked at 45 mA, the temperature tuning coefficient is about 0.115 nm per degree.

Current modulation

In the emission spectra modulation strategy, the center wavelength is roughly positioned around the selected absorption line through temperature control. In this case, taking consideration of both ambient temperature and control stability the temperature is locked at 18°C. With a

constant temperature, an increasing driving current moves the emitting spectrum of laser to higher wavelength. The current tuning coefficient is not a constant value under different temperature and the average value is about 0.0173 nm per micro ampere from 18 °C to 26 °C. The emission wavelength can be tuned from 1.6536 to 1.6552 μm for different temperatures and driving currents as shown in Fig. 5a. As the repeatability test, the current and temperature are kept constant as 40 mA and 18 °C focusing on the selected absorption wavelength. The intensity error was kept recording during 100 min and 10 peak errors in each 10 min are extracted as shown in Fig. 5b. The largest intensity amplitude error is 0.079, indicating a less than 0.1% amplitude fluctuation.

2f harmonic signals extraction

Experiments were carried out to derive the extraction performance of the orthogonal lock-in amplifier. During the experiment, the gas sample was continuously pumped into the chamber with a certain gas flow. An exhaust pipe was installed on the other side of the chamber to eliminate excess gas and maintain constant pressure. Three gas samples with a concentration of 100 ppm, 0.8% and 4% are prepared. To ensure result accuracy, the gas samples used for gas distribution were 5000 ppm methane with 2% uncertainty and 99.999% pure N_2 . In order to avoid operation errors caused by the external pressure difference, dynamic gas distribution was used instead of static injection distribution. The different concentrations of methane samples required were obtained by mixing the two standard gas samples mentioned above through a mass flow meter (MT50-3G). The peak to peak voltage amplitude of second-order harmonic signal shown in Fig. 6a and the extraction error (relative to the mean value) are shown in Fig. 6b. The results demonstrate that the developed orthogonal lock-in amplifier can effectively extract the desired signal and the relative extraction errors are 0.77%, 0.56%, and 0.55% for 100 ppm, 0.8% and 4%, respectively. This suggests a desired stability of the orthogonal lock-in amplifier and this performance could be further improved by increasing the integration time.

Control platform based on LabVIEW

The self-developed laser driving module and digital orthogonal lock-in amplifier based on LabVIEW platform is applied to driving the laser and receiving the original detected data. Other than some necessary hardware components such as a the DAQ, the digital driving and controlling modules effectively optimized the sensor size. Compared with the reported temperature control realized by hardware PID,^[17,19] errors caused by temperature drift of hardware device and related complex feedback compensation circuit can be avoided. The fuzzy PID algorithm is realized to enhance the laser control performance, such as response time, temperature stability, and so on. Compared with traditional signal processing modules realized by the

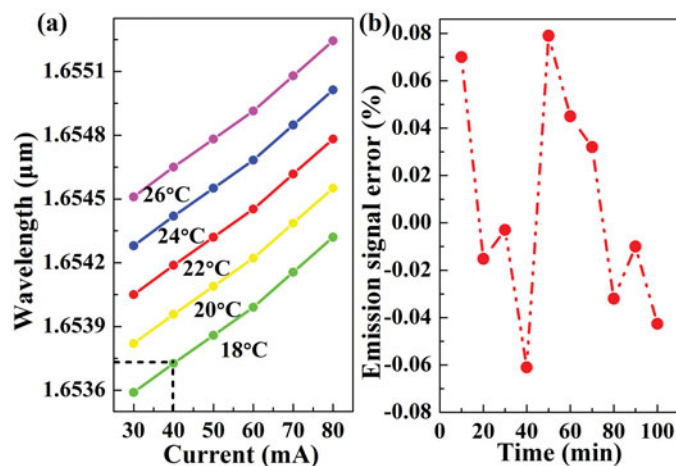


Figure 5. Emission spectra performance test for optimized driving condition selection. (a) Center wavelength versus the laser temperature and injection current. (b) Intensity error at 40 mA and 18 °C.

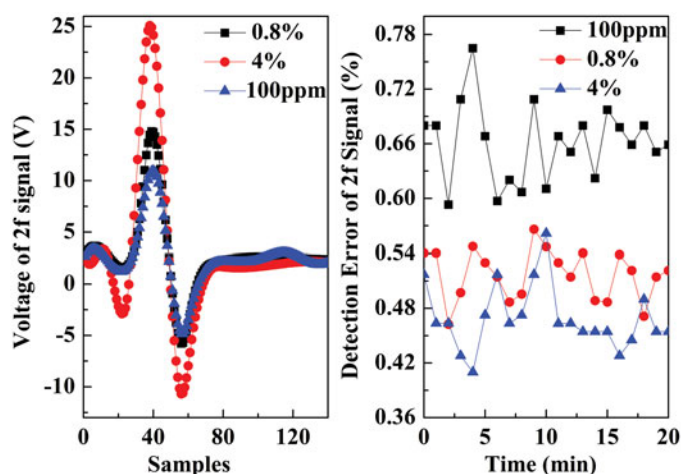


Figure 6. Function verification of self-developed lock-in amplifier harmonic extraction ability. (a) Extracted 2f harmonic signals results and (b) detection errors under 4%, 0.8% and 100 ppm methane.

microprocessor-like DSP chip, the self-developed control module on LabVIEW platform saves the hardware cost and enhances the flexibility of this system according to the online control board with adjustable parameters, like filter bandwidth, calibration parameters, and sampling frequency. With another laser with different central wavelength, this digital control platform can be used to measure some other gas component.

Besides the driving and real-time feedback, both first-order and second-order harmonic signals are extracted using the self-developed orthogonal lock-in amplifier. These functions are realized as a calculation daemon using a relative lower priority thread in kernel. The first-order harmonic signal is extracted and used to automatically calibrate the central wavelength drift caused by application environmental influence. The second-order harmonic signal is extracted and converted to the concentration value directly using the fitting formula. In addition, an internal additional display module is added in the background program to observe the real-time voltage of extracted second-order harmonic signal.

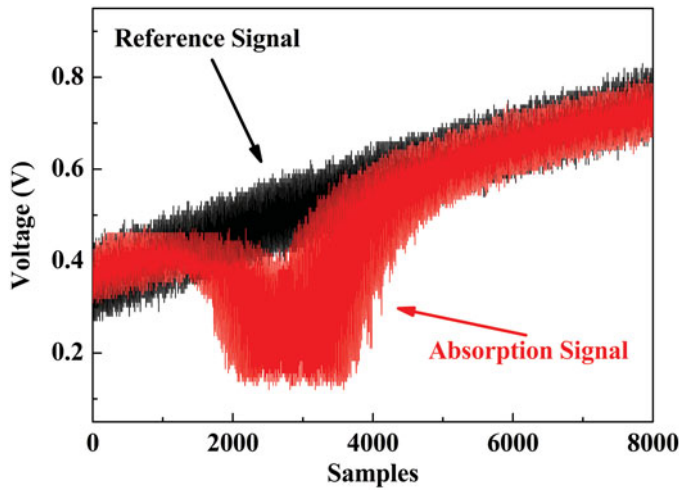


Figure 7. Extraction of the signal before processing for calibration verification. Measured waveforms of the original input absorption and reference signals before digital signal processing.

Experiment and calibration

Calibration and data fitting

In the data sampling of DAQ, the reference and detection signals after absorption in 30 cm gas cell were sampled, respectively. The differential 2f harmonic signal, which includes gas concentration information, was observed from the display module as shown in Fig. 7. The measured waveforms of absorption and reference signals are represented by red and black points, respectively. When the ramp wave scanned across the methane absorption spectrum, an obviously reduced section was observed, because of the absorption effect. For easy observation, this experiment was carried out using 12% methane, and the output voltage was directly measured from the detector without any signal processing.

Besides the rough assessment of different gas concentration measurement results, the amplitude of the 2f harmonic signal was directly proportional to gas concentration, which is in accordance with the TDLAS theory. In order to determine the relationship between the measured amplitude of extracted 2f harmonic signal and gas concentration, experiments under different gas concentrations were carried out. In accordance with Beer-Lambert law, the experimental results should show an exponential relationship. However, in the low concentration region, a linear fitting can be applied as shown in Fig. 8a. The voltage signal is the output through amplifier of the difference between reference and absorption signal. During the experiment, each sample was held for more than 10 min, and the average value was used to set up the calibration formula, shown in Fig. 8b. According to the experimental results, the maximum detection error was less than 3% at gas concentration higher than 100 ppm. With further decrease of gas concentration, the detection error sharply increased. The relationship between the extracted voltage signal and gas concentration can be expressed as formula 4.

$$C_{CH_4} = (V_{2f} - 1.19183)/0.08637 \quad (4)$$

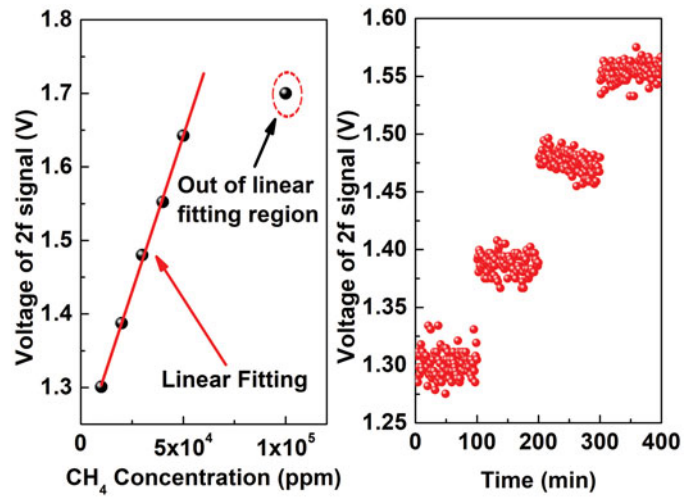


Figure 8. Dot plots and fitting curves for the extracted signal with methane concentration. (a) Fitted curve of relationship between 2f signal amplitude and methane concentration; (b) voltage value sampled of 2f signal in the low absorption region.

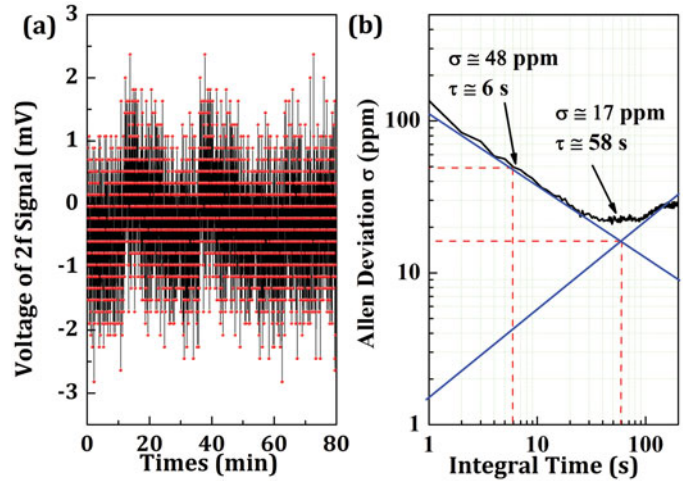


Figure 9. Limit of detection. (a) Relative detection error under 0 ppm methane; (b) Allan deviation analysis.

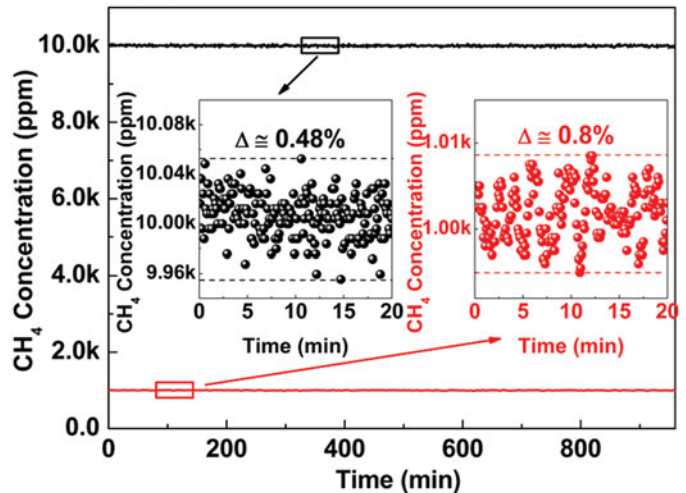


Figure 10. Stability detection. Stability test of methane at 1×10^3 ppm and 1×10^4 ppm during 12 hr.

Table 1. Comparison with reported methane detection system based on quantum cascade lasers and interband cascade lasers.

Refs	Source	Absorption length(m)	Center wavelength (um)	Limit of detection (ppm)	Cost
[28]	QCL	76	7.5	40 ppb	High
[29]	ICL	16	3.3	44 ppb	High
This article	DFB laser	0.3	1.65	48 ppm	Low

Table 2. Comparison with reported methane detection system based on similar design structure.

Refs.	Temperature control method and accuracy	Signal process method	Absorption length
[23]	PID based on digital signal processor $\pm 0.1^\circ\text{C}$, 66 s	Phase-tuned Lock-in amplifier	20 cm (no reflective cell)
This article	Fuzzy PID based on LabVIEW $\pm 0.018^\circ\text{C}$, 9 s	Orthogonal Lock-in amplifier	30 cm (single reflective cell)

Limit of detection

To assess the lower limit of detection, firstly the gas chamber was cleaned with pure nitrogen. Then, the methane mass flow was increased to 50 ppm and the gas flow was maintained at a small value after obtaining a stable record. During a period of 80 min, the sampled amplitude frequency of the extracted 2f signal was 10 Hz, and measured results are shown in Fig. 9a. The fluctuation range for sampled 2f signal voltage was ± 3 mv. Based on the experimental results, Allan deviation was calculated to analyze the stability and theoretical detection limit of the detection system. Allan deviation was plotted on a log-log scale versus averaging time τ as shown in Fig. 9b. The plot indicated a measurement precision of ~ 48 ppm with a ~ 6 s averaging time. The white noise was effectively suppressed at an integration time of 6 s. Meanwhile, the slope of Allan deviation was negative. With increasing averaging time, a measurement precision of ~ 17 ppm and a ~ 58 s averaging time were obtained at the intersection point of positive and negative slope; the main noise came from the temperature drift of the detection system. According to the above analysis, a relatively long integration time surely improves detection performance but yields a slower response. In *in-situ* application, the integration time can be adjusted through the control board of the LabVIEW platform to achieve optimal detection performance.

Detection stability

In stability experiments, the gas sample distributed by mass flow kept flushing with a low flow rate to ensure stable and accurate methane concentration in the chamber. As examples, low (1×10^3 ppm) and relatively high (1×10^4 ppm) concentrations were distributed, and data were recorded until stable reading. The experiments lasted for more than 12 hr. Because of system noise and interference, there were acceptable fluctuations of about 0.8% and 0.48% on 1×10^3 ppm and 1×10^4 ppm, as shown in Fig. 10, respectively.

Comparison and discussion

As exhibited in Table 1, the design structure and performance of this near-infrared detection sensor based on modulated DFB laser are compared with those of currently reported MIR detection devices using ICL and QCL. In the research of Qu et al.^[28] and Song et al.,^[29] a strong absorption line in MIR range and long light path using a commercial Herriott cell

effectively increases the detection performance. However, the strict working condition and high cost of those two sensors limit the actual application. Compared with the sensors developed based on QCL and ICL, the sensor developed in this article has a relatively low cost and simple structure. The size of developed gas cell is effectively decreased compared with the commercial one, such as $45 \times 11 \times 11 \text{ cm}^3$.^[29] In addition, the remote distributed detection which enhances the application ability in different conditions is realized.

As a comparison, the performances of this sensor and those reported with same DFB laser and TDLAS technology are listed in Table 2. The improvements of this sensor focus mainly on the high-robust temperature control and orthogonal lock-in amplifier. Firstly, in the temperature control, a fuzzy PID controller based on LabVIEW platform improves the control accuracy from $\pm 0.1^\circ\text{C}$ to $\pm 0.018^\circ\text{C}$. What's more, the fuzzy controller effectively decreases the response time from 66 s to 9 s. Secondly, the developed orthogonal lock-in amplifier is confirmed to be more convenient and efficient than a phase-tuned-type lock-in amplifier.^[23]

Conclusion

In this article, a low-cost, high-reliability methane-sensing system was designed and implemented. The DFB laser is modulated by a self-developed temperature controller and current modulator realized on the LabVIEW platform to scan across the related absorption spectrum. Experimental results indicated a satisfactory temperature fluctuation range of less than 0.01%. The laser's emitting wavelength varied linearly with temperature and injection current, and good operation stability for the laser was observed. A digital lock-in amplifier designed on the LabVIEW platform realized 2f harmonic signal extraction with an extraction error below 0.77%. According to gas experiments, the relative detection error was less than 3%. Allan deviation analysis revealed a lower limit of detection of about 48 ppm at 6 s integration time. Long-term stability experiments showed a fluctuation range of less than 0.8%. Besides improvement in cost-effective performance of this self-developed methane sensor, the driving module and signal processing module with real-time adjustment function achieved on the LabVIEW platform significantly improve the flexibility and scope of application. Furthermore, an embedded system can be used to replace the PC to achieve miniaturization.

Disclosure statement

No potential conflict of interest was reported by the authors.

Funding

This research was supported by the Basic Research Priorities Program of JiLin Province [No. 20170204019SF]; National Major Scientific Research Instrument and Equipment Development Project [No. 41527806]; “13th Five-Year” Science and Technology Project of Jilin Province Education Committee [No. JJKH20180573K], [JJKH20170240K]].

References

- Wong, K. W.; Fu, D.; Pongetti, T. J.; Newman, S.; Kort, E. A.; Duren, R.; Hsu, Y. K.; Miller, C. E.; Yung, Y. L.; Sander, S. P. Mapping CH₄: CO₂ Ratios in Los Angeles with CLARS-FTS from Mount Wilson, California. *Atmospheric Chemistry and Physics* **2015**, *15*, 241–252. doi: [10.5194/acp-15-241-2015](https://doi.org/10.5194/acp-15-241-2015).
- Simpson, I. J.; Rowland, F. S.; Meinardi, S.; Blake, D. R. Influence of Biomass Burning during Recent Fluctuations in the Slow Growth of Global Tropospheric Methane. *Geophysical Research Letters* **2006**, *33*, L22808. doi: [10.1029/2006GL027330](https://doi.org/10.1029/2006GL027330).
- Lang, N.; Macherius, U.; Wiese, M.; Zimmermann, H.; Röpcke, J.; van Helden, J. H. Sensitive CH₄ Detection Applying Quantum Cascade Laser Based Optical Feedback Cavity-Enhanced Absorption Spectroscopy. *Optics Express* **2016**, *24*, A536–A543. doi: [10.1364/OE.24.00A536](https://doi.org/10.1364/OE.24.00A536).
- Ye, W.; Li, C.; Zheng, C.; Sanchez, N. P.; Gluszek, A. K.; Hudzikowski, A. J.; Dong, L.; Griffin, R. J.; Tittel, F.K. Mid-infrared Dual-gas Sensor for Simultaneous Detection of Methane and Ethane Using a Single Continuous-wave Interband Cascade Laser. *Optics Express* **2016**, *24*, 16973–16985. doi: [10.1364/OE.24.016973](https://doi.org/10.1364/OE.24.016973).
- Salker, A. V.; Choi, N.-J.; Kwak, J.-H.; Joo, B.-S.; Lee, D. Thick Films of In, Bi and Pd Metal Oxides Impregnated in LaCoO₃ Perovskite as Carbon Monoxide Sensor. *Sensors Actuators B* **2005**, *106*, 461–467. doi: [10.1016/j.snb.2004.09.008](https://doi.org/10.1016/j.snb.2004.09.008).
- Wang, J. N.; Xue, Q. S.; Lin, G. Y.; Ma, Q. J. Mid-infrared Carbon Dioxide Sensor with Wireless and Anti-Condensation Capability for Use in Greenhouses. *Spectroscopy Letters* **2018**, *51*, 266–273. doi: [10.1080/00387010.2018.1468785](https://doi.org/10.1080/00387010.2018.1468785).
- Nagai, D.; Nishibori, M.; Itoh, T.; Kawabe, T.; Sato, K.; Shin, W. Ppm Level Methane Detection Using Micro-Thermoelectric Gas Sensors with Pd/Al₂O₃, Combustion Catalyst Films. *Sensors Actuators B* **2015**, *206*, 488–494. doi: [10.1016/j.snb.2014.09.059](https://doi.org/10.1016/j.snb.2014.09.059).
- Zhou, T. T.; Zhang, T.; Deng, J. N.; Zhang, R.; Zheng, L.; Wang, L. L. P-type Co₃O₄, Nanomaterials-Based Gas Sensor: Preparation and Acetone Sensing Performance. *Sensors Actuators B* **2017**, *242*, 369–377. doi: [10.1016/j.snb.2016.11.067](https://doi.org/10.1016/j.snb.2016.11.067).
- Zhou, T. T.; Zhang, T.; Zhang, R.; Deng, J. N.; Zheng, L.; Geyu, L.; Wang, L.L. Highly Sensitive Sensing Platform Based on ZnSnO₃, Hollow Cubes for Detection of Ethanol. *Applied Surface Science* **2017**, *400*, 262–268. doi: [10.1016/j.apsusc.2016.12.183](https://doi.org/10.1016/j.apsusc.2016.12.183).
- Ren, W.; Luo, L.; Tittel, F. K. Sensitive Detection of Formaldehyde Using an Interband Cascade Laser near 3.6 μm. *Sensors and Actuators B: Chemical* **2015**, *221*, 1062–1068. doi: [10.1016/j.snb.2015.07.078](https://doi.org/10.1016/j.snb.2015.07.078).
- Shemshad, J.; Aminossadati, S. M.; Kizil, M. S. A Review of Developments in Near infrared Methane Detection Based on Tunable Diode Laser. *Sensors and Actuators, B: Chemical* **2012**, *171*, 77–92. doi: [10.1016/j.snb.2012.06.018](https://doi.org/10.1016/j.snb.2012.06.018).
- Chen, C.; Newcomb, R. W.; Wang, Y. D. A Trace Methane Gas Sensor Using mid-Infrared Cascaded Laser at 7.5 μm. *Applied Physics B* **2013**, *113*, 491–501. doi: [10.1007/s00340-013-5473-7](https://doi.org/10.1007/s00340-013-5473-7).
- Goldenstein, C. S.; Spearrin, R. M.; Jeffries, J. B.; Hanson, R. K. Infrared Laser-Absorption Sensing for Combustion Gases. *Progress in Energy and Combustion Science* **2017**, *60*, 132–176. doi: [10.1016/j.peccs.2016.12.002](https://doi.org/10.1016/j.peccs.2016.12.002).
- Kamieniak, J.; Randviir, E. P.; Banks, C. E. The Latest Developments in the Analytical Sensing of Methane. *TrAC Trends in Analytical Chemistry* **2015**, *73*, 146–157. doi: [10.1016/j.trac.2015.04.030](https://doi.org/10.1016/j.trac.2015.04.030).
- Lohden, B.; Kuznetsova, S.; Sengstock, K.; Vaev, V. M.; Goldman, A.; Cheskis, S.; Palsdottir, B. Fiber Laser Intracavity Absorption Spectroscopy for In Situ Multicomponent Gas Analysis in the Atmosphere and Combustion Environments. *Applied Physics B* **2011**, *102*, 331–334. doi: [10.1007/s00340-010-3995-9](https://doi.org/10.1007/s00340-010-3995-9).
- Li, B.; Zheng, C. T.; Liu, H. F.; He, Q. X.; Ye, W. L.; Zhang, Y.; Pan, J. Q.; Wang, Y. D. Development and Measurement of a Near-Infrared CH₄ Detection System Using 1.654 μm Wavelength-modulated Diode Laser and Open Reflective Gas Sensing Probe. *Sensors and Actuators B* **2016**, *255*, 188–198. doi: [10.1016/j.snb.2015.11.037](https://doi.org/10.1016/j.snb.2015.11.037).
- Liu, T.; Wei, Y.; Song, G.; Hu, B.; Li, L.; Jin, G.; Wang, J.; Li, Y.; Song, C.; Shi, Z.; et al. Fiber Optic Sensors for Coal Mine Hazard Detection. *Measurement* **2018**, *124*, 211–223. doi: [10.1016/j.measurement.2018.03.046](https://doi.org/10.1016/j.measurement.2018.03.046).
- Lin, Y. X.; Wu, Q.; Li, W.; She, M. J.; Li, S. L. Application of Differential Optical Absorption Spectroscopy to Geological Logging. *Optics and Precision Engineering* **2013**, *21*, 3037–3042. doi: [10.3788/OPE.20132112.3037](https://doi.org/10.3788/OPE.20132112.3037).
- Zheng, C. T.; Huang, J. Q.; Ye, W. L.; Lv, M.; Dang, J. M.; Cao, T.S.; Chen, C.; Wang, Y.D. Demonstration of a Portable near-infrared CH₄ Detection Sensor Based Ontunable Diode Laser Absorption Spectroscopy. *Infrared Physics & Technology* **2013**, *61*, 306–312. doi: [10.1016/j.infrared.2013.08.006](https://doi.org/10.1016/j.infrared.2013.08.006).
- Cao, Y.; Sanchez, N. P.; Jiang, W.; Griffin, R. J.; Xie, F.; Hughes, L. C.; Zah, C. E.; Tittel, F. K. Simultaneous Atmospheric Nitrous Oxide, Methane and Water Vapor Detection with a Single Continuous Wave Quantum Cascade Laser. *Optics Express* **2015**, *23*, 2121–2132. doi: [10.1364/OE.23.002121](https://doi.org/10.1364/OE.23.002121).
- Manfred, K. M.; Ritchie, G. A. D.; Lang, N.; Röpcke, J.; van Helden, J. H. Optical Feedback Cavity-Enhanced Absorption Spectroscopy with a 3.24 m Interband Cascade Laser. *Applied Physics Letters* **2015**, *106*, 221106. doi: [10.1063/1.4922149](https://doi.org/10.1063/1.4922149).
- Li, G. L.; Sui, Y.; Dong, M.; Ye, W. L.; Zheng, C. T.; Wang, Y. D. A Carbon Monoxide Detection Device Based on Mid-infrared Absorption Spectroscopy at 4.6 μm. *Applied Physics B* **2015**, *119*, 287–296. doi: [10.1007/s00340-015-6056-6](https://doi.org/10.1007/s00340-015-6056-6).
- Zheng, C. T.; Ye, W. L.; Huang, J. Q.; Cao, T. S.; Lv, M.; Dang, J. M.; Wang, Y. D. Performance Improvement of a Near-infrared CH₄ Detection Device Using Wavelet-Denoising-Assisted Wavelength Modulation Technique. *Sensors and Actuators B* **2014**, *190*, 249–258. doi: [10.1016/j.snb.2013.08.055](https://doi.org/10.1016/j.snb.2013.08.055).
- Dang, J. M.; Yu, H. Y.; Sun, Y. J.; Wang, Y. D. A CO Trace Gas Detection System Based on Continuous Wave DFB-QCL. *Infrared Physics & Technology* **2017**, *82*, 183–191. doi: [10.1016/j.infrared.2016.12.012](https://doi.org/10.1016/j.infrared.2016.12.012).
- Anjos, J. M. S.; Coracini, G. K.; Villani, E. A Proposal and Verification of a Software Architecture Based on LabVIEW for a Multifunctional Robotic End-Effector. *Advances in Engineering Software* **2013**, *55*, 32–44. doi: [10.1016/j.advengsoft.2012.09.004](https://doi.org/10.1016/j.advengsoft.2012.09.004).
- Wang, J. N.; Niu, X. T.; Zheng, L. J.; Zheng, C. T.; Wang, Y. D. Visual Programming in the Wild: A Survey of LabVIEW Programmers[F]. *Sensors* **2016**, *16*, 1941. doi: [10.3390/s16111941](https://doi.org/10.3390/s16111941).
- Rieker, G. B.; Jeffries, J. B.; Hanson, R. K. Calibration-free Wavelength-Modulation Spectroscopy for Measurements of Gas Temperature and Concentration in Harsh Environments. *Applied Optics* **2009**, *48*, 5546–5560. doi: [10.1364/AO.48.005546](https://doi.org/10.1364/AO.48.005546).
- Qu, S. M.; Wang, M.; Li, N. Mid-Infrared Trace CH₄ Detector Based on TDLAS-WMS. *Guang Pu Xue Yu Guang Pu Fen Xi* **2016**, *36*, 3174–3178. doi: [10.3964/j.issn.1000-0593\(2016\)10-3174-05](https://doi.org/10.3964/j.issn.1000-0593(2016)10-3174-05).
- Song, F.; Zheng, C.; Yan, W.; Ye, W.; Wang, Y.; Tittel, F. K. Interband Cascade Laser Based Mid-infrared Methane Sensor System Using a Novel Electrical-domain Self-adaptive Direct Laser Absorption Spectroscopy (SA-DLAS). *Optics Express* **2017**, *25*, 31876. doi: [10.1364/OE.25.031876](https://doi.org/10.1364/OE.25.031876).